An Efficient Method for Frequency-Domain Simulation of Short Channel MOSFET Including the Non-Quasistatic Effect

Kyu-Il Lee*, Chanho Lee†, Hyungsoon Shin‡, Young June Park*, and Hong Shick Min*
*School of Electrical Engineering and Computer Science, Seoul National University, Seoul 151–744, Republic of Korea
E-mail: macjr@bawi.org, Phone: (+82-2) 880-7285, Fax.: (+82-2) 882-4658
†School of Electronics Engineering, Soongsil University, Seoul 156–743, Republic of Korea
‡Department of Information Electronics Engineering, Ewha Womans University, Seoul 120–750, Republic of Korea

Abstract— **In this paper, we propose an efficient method for the harmonic balance analysis of the short channel MOSFET including the non-quasistatic effect. Our method is based on the charge-sheet model in the linear region and assumes that the saturation region is modulated by the external voltage instantaneously. By comparing with the current responses under large signal conditions obtained from the time-dependent two-dimensional simulator (*MEDICI*), it is confirmed that the proposed method is efficient and accurate for the frequency-domain analysis of the short channel MOSFET in the 0.1 μm regime.**

I. Introduction

It becomes more important to obtain an accurate distortion model of the MOSFET devices operating under large signal conditions as the CMOS technology plays a key role in the recent RF applications [1]. The distortion of the signal mainly arises from the nonlinear characteristics of the MOSFET device. In order to derive an accurate model describing the nonlinear effects, the short channel effects should be properly considered such as the lateral field effect on the mobility, the channel length modulation, and the velocity saturation effect. Also, the non-quasistatic (NQS) effect in the carrier transport should be included as the operating frequency is increased.

The short channel effects have been taken into account in the device- and circuit-level simulators. The time-domain device simulation method may be the first choice to this end. But when there exist multi-tone inputs to the device with large common period, too many integration steps are needed to follow the input signal. The harmonic balance (HB) technique for the semiconductor device was first implemented in *PISCES-HB* [2], the two-dimensional device simulator, in order to overcome this demerit [3]. However, this approach requires to solve the system equation with $3N(2H+1)$ unknowns, where '3' comes from potential, electron and hole concentrations, N is the total number of internal nodes and H is the harmonic truncation number, which still may result in tremendous computational time as N increases in the two-dimensional simulation. The models for the circuit-level simulation such as SPICE may be used [4], [5], but the harmonic distortion phenomenon due to the non-quasistatic effect cannot be easily considered since they are mainly based on the time-domain and quasistatic (QS) simulations.

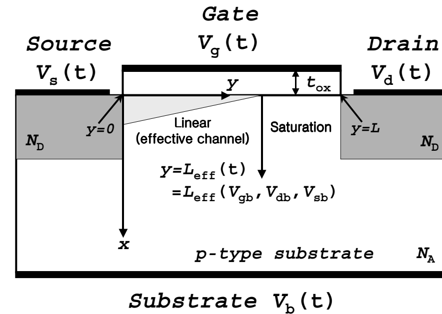

Fig. 1. Notations: $V_{ij} = V_i - V_j$ $(i, j = b, g, s, d)$

In this viewpoint, we proposed a frequency-domain simulation method for the analysis of the long channel MOSFET [6] employing the one-dimensional charge-sheet approximation (CSA), the frequency-domain simulation via the harmonic balance technique, and the NQS model proposed in [7]. The applicability and efficiency were tested and confirmed to show that our method is not only computationally efficient but also physically reasonable.

As an extension of our previous work, we have developed a short channel MOSFET model including the modulation of the effective channel length according to the external biases. We will show that the method achieves an accurate frequency-domain analysis for the short channel MOSFET with minimum numerical burden.

II. Short Channel MOSFET Model

Fig. 1 shows the notations used in our nMOSFET model. Most of the notations follow the conventional definitions except for L_{eff}, the effective channel length, which is defined as the length of the linear region in the channel and is instantaneously modulated by the external biases.

A. Quasistatic Part

The normalized charge density per unit area at some point in the channel, which is obtained from the integration of the electron concentration in the vertical direction, can be

 0-7803-7826-1/03/$17.00 © 2003 IEEE

simplified as [7], [8]

$$q_{\mathrm{e}} = -\frac{q}{C_{\mathrm{ox}}}\int_0^{X_{\mathrm{d}}} n(x)dx = V_{\mathrm{gb}} - V_{\mathrm{FB}} - \phi_{\mathrm{s}} + \eta\sqrt{\phi_{\mathrm{s}}} \overset{\mathrm{let}}{=} -\alpha\left(\phi_{\mathrm{s}} + \beta + V_{\mathrm{t}}\right), \quad (1)$$

where C_{ox} is the oxide capacitance per unit area, X_{d} is the depletion width in the channel region given as $\sqrt{2\epsilon_{\mathrm{si}}\phi_{\mathrm{s}}/qN_{\mathrm{A}}}$, V_{FB} is the flat-band voltage, $\eta = \gamma\left(A\epsilon_{\mathrm{si}}V_{\mathrm{ds}}/qN_{\mathrm{A}}L^2 - 1\right)$, V_{t} is the thermal voltage, γ is the body factor, N_{A} is the substrate doping concentration, and A is the linearization factor for the lateral field gradient term (usually $0.7 \leq A \leq 1$) [9]. In the derivation of (1), the contribution of the bulk charges and the lateral field non-uniformity are simplified by some mathematical treatments of the Poisson equation. Also, we divide the physical channel region into two parts: the linear and the saturation regions. The boundary condition at channel ends determines the linearization coefficients α and β in (1), which are regarded as quasistatic quantities.

The electron current under the CSA considering both drift and diffusion components in the linear region can be expressed as [7]

$$\frac{I(y)}{WC_{\mathrm{ox}}} = \left(V_{\mathrm{t}}\frac{\partial q_{\mathrm{e}}}{\partial y} - q_{\mathrm{e}}\frac{\partial \phi_{\mathrm{s}}}{\partial y}\right) = \frac{\mu_{\mathrm{n}}\alpha}{2}\cdot\frac{\partial}{\partial y}\left[(\phi_{\mathrm{s}} + \beta)^2\right], \quad (2)$$

where μ_{n} includes the velocity saturation effect as

$$\mu_{\mathrm{n}} = \mu_{\mathrm{eff}} \Big/ \sqrt{1 + \left(\bar{\mathbf{E}}/E_{\mathrm{c}}\right)^2}, \quad (3)$$

where E_{c} is the critical field intensity given as $v_{\mathrm{sat}}/\mu_{\mathrm{eff}}$, $\bar{\mathbf{E}}$ is the averaged lateral field given as $\left(\phi_{\mathrm{s}}(L_{\mathrm{eff}}) - \phi_{\mathrm{s}}(0)\right)/L_{\mathrm{eff}}$, v_{sat} is the electron saturation velocity, and $\phi_{\mathrm{s}}(L_{\mathrm{eff}})$ and $\phi_{\mathrm{s}}(0)$ are the surface potentials at the drain-side and the source-side ends of the effective channel, respectively. The effective mobility, μ_{eff}, is a function of the substrate doping concentration and the vertical field, thus V_{gb}.

Based on the CSA in the linear region, an analytic equation for the quasistatic surface potential in the channel, $\phi_{\mathrm{s}}^{\mathrm{QS}}$, can be obtained by letting the time-independent current continuity equation, $WC_{\mathrm{ox}}\partial q_{\mathrm{e}}/\partial t = \partial I/\partial y$, be zero with (2):

$$\phi_{\mathrm{s}}^{\mathrm{QS}}(y) + \beta = -\sqrt{(m^2 - n^2)\, y/L_{\mathrm{eff}} + n^2}, \quad (4)$$

where $m = \phi_{\mathrm{s}}(L_{\mathrm{eff}}) + \beta$ and $n = \phi_{\mathrm{s}}(0) + \beta$. The surface potential at the source-side end of the channel is calculated iteratively from the well-known MOSFET charge equation considering the lateral field gradient term by the same way as in (1). The quasistatic (QS) current, I_0, can then be written as

$$I_0 = WC_{\mathrm{ox}}\mu_{\mathrm{n}}\left(m^2 - n^2\right)/2L_{\mathrm{eff}}. \quad (5)$$

The saturation surface potential (ϕ_{sat}) for the start of the current saturation can be obtained by letting $\phi_{\mathrm{sat}} = \phi_{\mathrm{s}}(L_{\mathrm{eff}})$, $\partial I_0/\partial\phi_{\mathrm{s}}(L_{\mathrm{eff}}) = 0$ and $L_{\mathrm{eff}} = L$ in (5) and the saturation channel potential ($V_{\mathrm{ds,sat}}$) can be calculated from $V_{\mathrm{ds,sat}} = \phi_{\mathrm{sat}} - \phi_{\mathrm{s}}(0)$. It is generally accepted that the channel potential at the end of the effective channel is V_{ds} when the device is operating in the linear region and is pinned at $V_{\mathrm{ds,sat}}$ in the saturation region. This simple approach evokes a discontinuity problem in the time derivative of the channel potential at the end of the channel, which degrades the stability of numerical approach. To avoid this problem, a smoothing function [5] is used to guarantee the smooth transition of physical quantities between the linear and saturation regions while maintaining the pinch-off characteristic of the channel potential at the end of the effective channel when there exists the timing change in the drain bias. The channel potential at the effective channel end using the smoothing function is then written as

$$V_{\mathrm{cb,eff}}(V_{\mathrm{ds}}) = V_{\mathrm{ds}} \Big/ \sqrt[2\kappa]{1 + \left(V_{\mathrm{ds}}/V_{\mathrm{ds,sat}}\right)^{2\kappa}} + V_{\mathrm{sb}}, \quad (6)$$

where κ is an arbitrarily chosen integer number (2 in this work), which does not give a sensitive result. Then the surface potential at the drain-side end of the channel can also be determined from the MOSFET charge equation by changing $\phi_{\mathrm{s}}(0)$ to $\phi_{\mathrm{s}}(L_{\mathrm{eff}})$ and V_{sb} to $V_{\mathrm{cb,eff}}$.

The surface potential has been reported to have the following form in the saturation region ($L_{\mathrm{eff}} \leq y \leq L$) [9], [10]:

$$\phi_{\mathrm{s}}(y) = a + b\sinh\left((y - L_{\mathrm{eff}})/l\right) + c\sinh\left((L - y)/l\right), \quad (7)$$

where the characteristic length l ($= \sqrt{3t_{\mathrm{ox}}X_{\mathrm{j}}}$, X_{j}: junction depth) approximates the spreading effect of the mobile charges into the bulk direction [11]. The effective channel length (hence a, b, and c also) can be determined from both the continuity conditions of the potential, field (first derivative), and charge density (second derivative) at $y = L_{\mathrm{eff}}$ and the properly-chosen boundary condition on $y = 0$ and $y = L$.

In the current saturation region, we assume that the effective channel length responds instantaneously to the timing change of the external biases, i.e.,

$$L_{\mathrm{eff}}(t) = L_{\mathrm{eff}}\left(V_{\mathrm{ext}}(t), dV_{\mathrm{ext}}(t)/dt, \cdots\right) \simeq L_{\mathrm{eff}}\left(V_{\mathrm{ext}}\right). \quad (8)$$

B. Non-Quasistatic Part

Now, let us consider the NQS component of the surface potential. The carrier transport in the saturation region can be regarded as quasistatic since the carriers have very high velocity there. Thus the non-quasistatic component for $0 \leq y \leq L_{\mathrm{eff}}$ can be expressed as

$$\phi_{\mathrm{s}}^{\mathrm{NQS}}(y,t) = \sum_{m=1}^{M}\phi_m(t)\sin\left(m\pi y/L_{\mathrm{eff}}(t)\right), \quad (9)$$

where M is the truncation number of the spatial sine expansion.

The time-dependent current continuity equation with (1) yields our master equation including both the QS and NQS components as follows:

$$\frac{\partial}{\partial t}\left[\alpha\left(\phi_{\mathrm{s}} + \beta + V_{\mathrm{t}}\right)\right] + \frac{\mu_{\mathrm{n}}\alpha}{2}\cdot\frac{\partial^2}{\partial y^2}\left[(\phi_{\mathrm{s}} + \beta)^2\right] = 0, \quad (10)$$

where $\phi_{\mathrm{s}}(y,t) = \phi_{\mathrm{s}}^{\mathrm{QS}}(y,t) + \phi_{\mathrm{s}}^{\mathrm{NQS}}(y,t)$. Our solution vector for the above master equation consists of the Fourier coefficients of $\phi_{\mathrm{m}}(t)$ represented as [3]

$$\phi_{\mathrm{m}}(t) = \phi_{\mathrm{m,0}}^R + \sum_{h=1}^{H}\left(\phi_{\mathrm{m,h}}^R\cos\omega_{\mathrm{h}}t - \phi_{\mathrm{m,h}}^I\sin\omega_{\mathrm{h}}t\right), \quad (11)$$

 0-7803-7826-1/03/$17.00 © 2003 IEEE

TABLE I
DEVICE PARAMETERS FOR $0.18\mu\mathrm{m}$ MOSFET SIMULATION

parameter	W/L	N_{A}	t_{ox}	X_{j}	v_{sat}
value	1.8/0.18	5×10^{17}	39	0.25	1.035×10^{7}
unit	[μm]	[cm^{-3}]	[Å]	[μm]	[cm/sec]

where H is the number of considered harmonic components truncated from infinite harmonics. Our goal is to satisfy the master equation by adjusting the coefficients in (11) through the Newton-Raphson method [12]. The frequency-domain formulation is the same as in the long channel case except for the normalized space-sampling points (nodes in the linear region; $0 \leq y \leq L_{\mathrm{eff}}$) varying with time. As we are to solve the master equation only in the channel region with the saturation point modulated by the external biases, we consider equally-spaced internal nodes at each time-sampling point.

For the calculation of the source and drain terminal currents, the displacement current is also included for the charging current by the junction capacitance.

III. SIMULATION RESULTS AND DISCUSSION

Table I shows the device parameters used in the simulations. These parameters are from the SPICE model parameters of 0.18 μm nMOSFET device produced by *Dongbu Electronics Company*.

Comparisons of results are made with *MEDICI* [13], the well-tuned two-dimensional analysis tool. Our method needs no more than six Newton steps for the following simulations to an acceptable convergence criterion, which shows the efficiency of our method for all cases.

A. DC analysis

We checked dc I–V characteristics in order to validate the QS part of our model. First, from Fig. 2(a), it can be noticed that the new model predicts precise I_{d}–V_{g} characteristics from the subthreshold to the strong inversion conditions. Second, comparisons of I_{d}–V_{d} characteristics drawn in Fig. 2(b) show that our model is accurate and continuous in the whole operating condition of the MOSFET, from linear to saturation condition. Furthermore, g_{ds} shows no discontinuity around $V_{\mathrm{ds}} = 0$ V, which has been the problem of some circuit simulators [5] using a source-referenced model and simple consideration of lateral field contribution to the carrier mobility.

B. AC analysis

Fig. 3 depicts the harmonic distortion components of the drain current for $V_{\mathrm{gb}} = 1.5$ V and a large-signal single-tone (100 GHz) input on the drain as $V_{\mathrm{ds}} = 1.5 + 1.5\sin(2\pi \times 10^{11}t)$ V. The QS harmonic distortion components are generated by the nonlinear behavior of the system and the NQS harmonic distortion components are from both the nonlinearity and the NQS effect in the carrier transport. It can be seen from Fig. 3 that the NQS components are important for the distortion components.

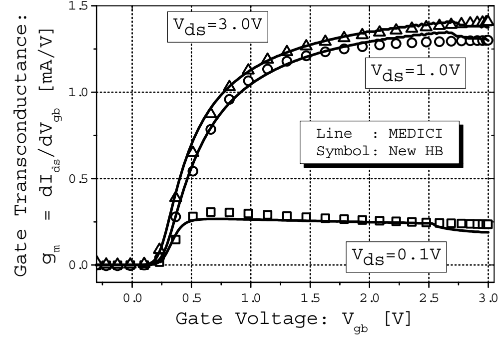

(a)

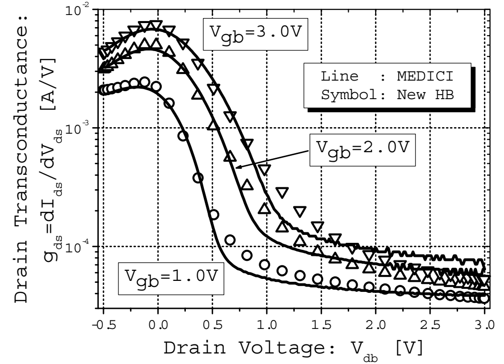

(b)

Fig. 2. Comparison of (a) gate transconductance g_{m} and (b) drain-source transconductance (output conductance) g_{ds} of a 0.18μm MOSFET

The time-varying periodic inputs on gate or drain are shown in Fig. 4. Because our simulation is performed in the frequency domain, Fourier coefficients of 50 harmonics of the input are calculated to represent the input waveform which needs 101 time-sampling points. For the purpose of imposing the same numerical burden, one period of input is sliced with 101 time samples in *MEDICI* simulation.

The source and drain currents are drawn in Figs. 5(a) and 5(b) with respect to time, when ramp signals are exerted on the gate with the input frequencies of 1 GHz and 50 GHz. While the source and drain currents are almost identical for the case of 1 GHz, there exists an appreciable difference between two currents for the input of 50 GHz. When the gate voltage is raised, the source current leads the drain current because it takes a finite time for electrons to form the inversion layer. The reverse action occurs for the case of ramp down of the gate voltage. This phenomenon is a typical characteristic of the NQS effect aroused by a high frequency input.

For a different circuit configuration, the simulation result for a sawtooth-shaped input on the drain is shown in Fig. 6. Again good agreement for both simulations is obtained. It should be noticed that the charging current for the junction capacitance is properly implemented.

 0-7803-7826-1/03/$17.00 © 2003 IEEE

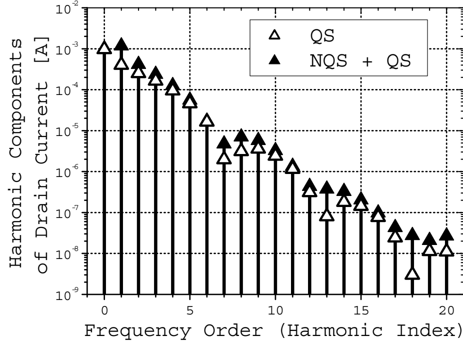

Fig. 3. Harmonic distortion of drain current generated by dc *plus* single-tone drain voltage

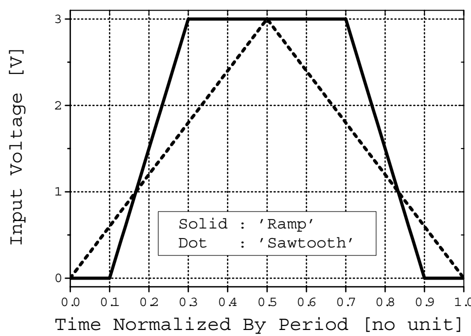

Fig. 4. Ramp and sawtooth signals for input: time scale is normalized by period.

IV. Conclusion

Our new model yields not only an efficient simulation of the short channel MOSFET but also physically accurate results when harmonic and periodic inputs are present. Our model may be a good basis for the HB analysis to understand the effects of the various physical mechanisms and the device structures on the nonlinear distortions and noises with a small computation load and we are expecting to extend our model to the circuit environments.

Acknowledgment

The authors appreciate the support of the *National Research Laboratory Project of the Ministry of Science and Technology* and the *Brain Korea 21 Project*. This work has also been supported by *A Collaborative Project for Excellence in System IC Technology*.

References

[1] T. A. M. Kevenaar and E. J. W. ter Maten, *Proc. of SISPAD*, pp. 7–10, Sep. 1999.
[2] B. Troyanovsky, Z. Yu, and R. W. Dutton, *Proc. of SISPAD*, pp. 114-117, Sep. 1995.
[3] B. Troyanovsky, *Large Signal Frequency Domain Device Analysis via the Harmonic Balance Technique*, Ph. D. Dissertation, Stanford Univ., Nov. 1997.
[4] A. R. Boothroyd, S. W. Tarasewicz, and C. Slaby, *IEEE Trans. on CAD*, vol. 10, pp. 1512–1529, Dec. 1991.
[5] K. Joardar, K. K. Gullapalli, C. C. McAndrew, M. E. Burnham, and A. Wild, *IEEE Trans. on ED*, vol. 45, pp. 134–148, Jan. 1998.

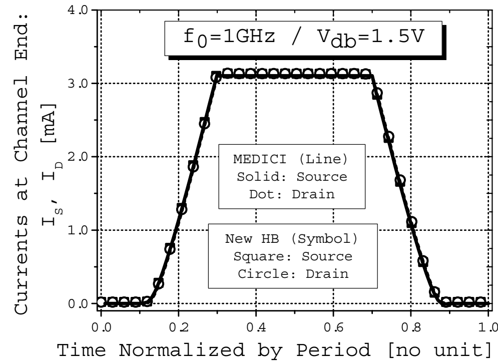

(a)

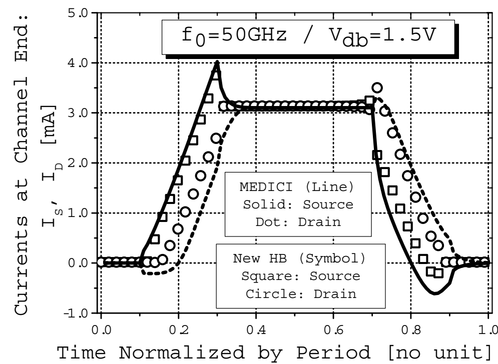

(b)

Fig. 5. Ramp input on gate: periods are (a) 1 nsec (1 GHz) and (b) 20 psec (50 GHz).

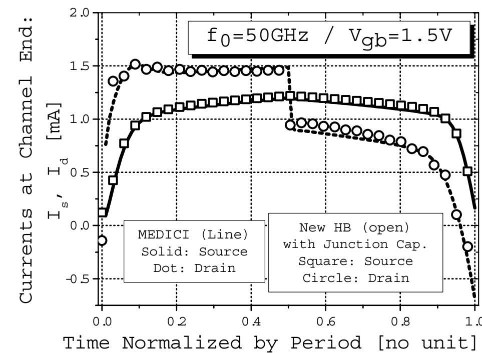

Fig. 6. Sawtooth-shaped input on drain: period is 20 psec (50 GHz).

[6] K. -I. Lee, et al., *IEEE Trans. on CAD*, vol. 20, pp. 867–876, Jul. 2001
[7] H. J. Park, *Charge-Sheet and Non-Quasistatic MOSFET Models for SPICE*, Ph. D. Dissertation, Univ. of California, Berkeley, Feb. 1989.
[8] M. Miura-Mattausch, U. Feldmann, A. Rahm, M. Bollu, and D. Savignac, *IEEE Trans. on CAD*, vol. 15, pp. 1–7, Jan. 1996.
[9] Z. Liu et al., *IEEE Trans. on ED*, vol. 40, pp. 86–95, Jan. 1993.
[10] K. W. Terrill, C. Hu, and P. K. Ko, *IEEE EDL*, vol. EDL-5, pp. 440–442, Nov. 1984.
[11] Y. Taur and T. H. Ning, *Fundamentals of Modern VLSI Devices*, pp. 156–158, Cambridge University Press, 1998.
[12] W. H. Press, S. A. Teukolsky, W. T. Vetterling, and B. P. Flannery, *Numerical Recipes in C++*, 2nd Edi., pp. 366–393, Cambridge University Press, 2002.
[13] *MEDICI User's Manual*, Avant! Corp., Feb. 2001.

 0-7803-7826-1/03/$17.00 © 2003 IEEE